TU Delft

Delft University of Technology

Development of a sustainable stabilized macadam road base using steel slag as supplementary cementitious material

Yang, Xinkui; Wu, Shaopeng; Chen, Boyu; Ye, Guang; Xu, Shi

DOI
10.1016/j.conbuildmat.2024.138566

Publication date
2024

Document Version
Final published version

Published in
Construction and Building Materials

Citation (APA)
Yang, X., Wu, S., Chen, B., Ye, G., & Xu, S. (2024). Development of a sustainable stabilized macadam road base using steel slag as supplementary cementitious material. *Construction and Building Materials*, *449*, Article 138566. https://doi.org/10.1016/j.conbuildmat.2024.138566

Important note
To cite this publication, please use the final published version (if applicable).
Please check the document version above.

Copyright
Other than for strictly personal use, it is not permitted to download, forward or distribute the text or part of it, without the consent of the author(s) and/or copyright holder(s), unless the work is under an open content license such as Creative Commons.

Takedown policy
Please contact us and provide details if you believe this document breaches copyrights.
We will remove access to the work immediately and investigate your claim.

This work is downloaded from Delft University of Technology.
For technical reasons the number of authors shown on this cover page is limited to a maximum of 10.

Green Open Access added to TU Delft Institutional Repository

'You share, we take care!' - Taverne project

https://www.openaccess.nl/en/you-share-we-take-care

Otherwise as indicated in the copyright section: the publisher is the copyright holder of this work and the author uses the Dutch legislation to make this work public.

Construction and Building Materials 449 (2024) 138566

Contents lists available at ScienceDirect

Construction and Building Materials

journal homepage: www.elsevier.com/locate/conbuildmat

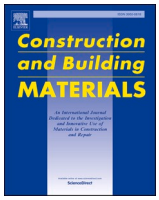

Development of a sustainable stabilized macadam road base using steel slag as supplementary cementitious material

Xinkui Yang [a], Shaopeng Wu [a], Boyu Chen [c], Guang Ye [c], Shi Xu [b,c,*]

[a] State Key Laboratory of Silicate Materials for Architectures, Wuhan University of Technology, Wuhan 430070, China
[b] School of Civil Engineering and Architecture, Wuhan University of Technology, Luoshi Road 122, Wuhan 430070, China
[c] Faculty of Civil Engineering and Geosciences, Delft University of Technology, Stevinweg 1, Delft 2628 CN, the Netherlands

ARTICLE INFO

Keywords:
Steel slag
Cement stabilized macadam
Water damage
Heavy metal ions

ABSTRACT

As the main waste product of iron and steel industry, steel slag possesses considerable cementitious activity, making it a promising alternative to cement in Cement Stabilized Macadam (CSM). However, CSM was inevitably exposed to groundwater and rainwater when served as the pavement base course, leading to concerns over poor early strength and potential pollutant leakage, which are the main factors that may hinder the widespread utilization of steel slag in CSM base. To address these issues, this study investigated the feasibility of using steel slag powder to produce CSM. Steel Slag Powder-Cement Stabilized Macadam (SSCSM) samples were prepared and the hydration products, microstructure, mechanical properties, water damage resistance and heavy metal ions leaching behavior were investigated. The results show that the nucleation effect of steel slag powder accelerates the early hydration, but the C-S-H produced by hydration is not sufficient to form a stable hydration product network, so the microstructure of SSCSM is looser than that of CSM. The addition of steel slag powder improved the shrinkage performance of SSCSM, and the mechanical properties and heavy metal ion leaching concentration of SSCSM meet the engineering application requirements when the steel slag powder replacement level does not exceed 30 %. It was also found that the addition of steel slag powder promoted the development of pores in SSCSM samples after dry-wet cycles, resulting in the reduction of water damage resistance. Compared with conventional CSM, the use of SSCSM can not only reduce 4 % of raw material cost and 23.5 % of equivalent CO_2 emission, but also mitigate the heavy metal ions leaching risk associated with steel slag, making it an effective and sustainable solution for steel slag recycling.

1. Introduction

Steel slag is a large-scale industrial solid waste stream generated by the iron and steel industry [1–3]. China produced 1.013 billion tons of crude steel in 2022, which resulted in the generation of more than 160 million tons of steel slag. Although steel slag is commonly recycled as aggregates in road engineering, its utilization rate in China remains below 30 % [4–9]. Large amounts of waste steel slag require significant land resources for storage. Moreover, the piling-up of steel slag poses a heavy metal leaching risk when exposed to natural water such as flood, rain, etc., which results in soil pollution, placing a significant burden on the environment [10–12].

Steel slag is primarily composed of C_2S and C_3S, which can form calcium silicate hydrates (C-S-H) when reacted with water, demonstrating the prospect to be utilized as cementitious materials [13–16]. However, compared to other industrial by-products that are commonly employed as supplemental cementitious material (SCM), such as blast furnace slag and fly ash, steel slag has lower hydration activity. Using steel slag as SCM will reduce early strength, which limits its applicability in cement-based materials [17–19]. Zhuang and Wang [20] investigated the hydration mechanism of steel slag's early hydration. They found that the pH of the blended cement paste's pore solution was lowered by steel slag, the formation and development of C-S-H were also inhibited, leading in a reduction of hydration rate.

It has been proven that activating steel slag is a reliable way to enhance its early hydration activity. Singh et al. [21] investigated the mechano-chemical activation of steel slag. Firstly, the steel slag was ground for 20 minutes, until its specific surface area reached 3590 cm^2/g. Next, sodium silicate and sodium sulfate were employed for chemical activation of steel slag powder (SSP). The findings

* Corresponding author at: School of Civil Engineering and Architecture, Wuhan University of Technology, Luoshi Road 122, Wuhan 430070, China.
E-mail address: xushi@whut.edu.cn (S. Xu).

https://doi.org/10.1016/j.conbuildmat.2024.138566
Received 12 January 2024; Received in revised form 29 July 2024; Accepted 30 September 2024
Available online 3 October 2024
0950-0618/© 2024 Published by Elsevier Ltd.

demonstrated that the hydration activity of SSP was largely improved after mechano-chemical activation, and the sample's 28-day compressive strength was enhanced by 12.64 %. Zhang et al. [22] added nano-SiO_2 to the SSP-cement cementitious system to enhance the concrete's early strength. The incorporation of nano-SiO_2 reduced the porosity of concrete and the hydration heat of cementitious system, and improved the hydration degree of steel slag.

A great deal of study has also been done to assess the risks of heavy metal leaching from steel slag [23,24]. Gan et al. [25] studied the leaching risk of steel slag asphalt mixture. The findings indicate that under acid rain, the leaching risks of heavy metal ions in steel slag would significantly increase, and the gradation and asphalt content are the primary factors influencing the leaching behavior of steel slag. Wang et al. [26] developed a kind of steel slag-based cementitious material and studied its leaching behavior of heavy metals. They found that hydration would change the leaching behavior of heavy metals. As the duration of the curing increased, the leaching concentration of Cr increased and the leaching concentration of Mn decreased. Sun et al. [27] utilized steel slag to produce SCM after mechanical activation and analyzed its heavy metals leaching risks. They found that wet grinding greatly raised the probability of heavy metal leaching and increased the leaching concentrations of Ti, Cr, Mn, and Zn in steel slag. The potential risk of steel slag in heavy metal leaching has aroused people 's concern about its safety and hindered its recycling and utilizing in engineering.

Cement stabilized macadam (CSM) is the most widely used semi-rigid base material in pavement engineering. It consists of cement and graded broken stone and is often used as the base course of high-grade pavement structures in China [28]. Traditional CSM uses cement and limestone as cementitious materials and aggregates, it raises the cost of the engineering while also consuming a lot of mineral resources. Therefore, if steel slag aggregates or SSP can be utilized for the production of CSM, the engineering cost of road base can be reduced. However, in engineering applications, CSM is prone to volume shrinkage due to water loss, and leads to shrinkage cracks in road base. The service life of the pavement structure will be limited due to the development of these cracks [29–31]. Considering that the reaction between f-CaO in steel slag particles and water can lead to poor volume stability [32], the utilization of SSP instead of cement in preparing CSM can not only mitigate the adverse effect of steel slag aggregates on the volume stability of road base materials but also reduce the carbon emissions generated by cement consumption and promote the recycling of steel slag. However, how to prepare the Steel Slag Powder-Cement Stabilized Macadam (SSCSM) and the effect of SSP on the mechanical performance, shrinkage performance and heavy metal leaching performance of base materials remain unclear.

This study investigated the potential use of SSP to replace cement in the manufacture of CSM. Firstly, the SSCSM mixture was designed and the cylinder samples and beam samples were prepared. The hydration chemical kinetics of SSCSM samples were investigated by hydration heat test. The microstructure and hydration product distribution of SSCSM samples were observed by scanning electron microscope (SEM). The elemental composition of hydration products was analyzed by energy dispersive spectrometer (EDS). Then, the mechanical properties and shrinkage properties of SSCSM were studied, and the water damage resistance of SSCSM was tested by dry-wet cycling test and X-ray computed tomography (X-CT). A column leaching testing setup was developed to simulate the leaching behavior of heavy metal ions in SSCSM during rainfall in Hubei Province, China. Finally, the economic and environmental benefits of SSCSM were compared. The findings of this paper establish a theoretical basis for the feasibility of utilizing steel slag in base course and offer a cleaner approach for the recycling of steel slag.

2. Materials and methods

2.1. Materials

The physical properties of P.I 42.5 Portland cement used in this study are shown in Table 1. SSP was provided by China Baowu Iron and Steel Group Co., Ltd., and the limestone aggregates were produced from a stone factory in Wuhan. The physical properties of limestone aggregates are shown in Table 2.

The results of X-ray fluorescence (XRF) test and X-ray diffraction (XRD) analysis of SSP are shown in Table 3 and Fig. 1(a). The XRF results show that the primary oxides of steel slag are CaO, Fe_2O_3, SiO_2 and Al_2O_3, which account for 83.46 % of the total components. The XRD results show that the steel slag's primary mineral components are olivine (γ-C_2S), β-larnite (β-C_2S) and hatrurite (C_3S). In addition, the mineral components of steel slag also contain srebrodolskite (C_2F), mayenite ($C_{12}A_7$), RO phase, quartz (SiO_2) and calcium aluminate (C_3A). RO phase is the solid solution formed by metal oxides such as MgO, MnO and FeO in steel slag at high temperature [33]. The cementitious composition of steel slag (β-C_2S and C_3S) is similar to that of cement, which provides a possibility for using SSP as cementitious material. The particle size distribution of SSP is shown in Fig. 1(b). The specific surface area of SSP is 467 m^2/kg, which is higher than that of cement (Table 1). The higher specific surface area helps to improve the early reactivity of SSP.

2.2. Mixture design and sample preparation

According to the Chinese standard JTG-T-F20–2015[34], the C-A-1 gradation can be used as the subbase gradation of expressway. Therefore, it is selected as the design gradation of SSCSM. According to the screening results of the aggregates, a gradation close to the grading median is designed, as shown in Fig. 2. The amount of cement and SSP is 5 % of the total weight of aggregate. Considering that high amount of SSP in SSCSM will significantly affect the mixture's early strength [26]. SSP was used to replace 10 wt%, 20 wt%, 30 wt% and 40 wt% of cement. As shown in Table 4.

The compaction test was carried out on mixtures with different SSP contents to obtain the maximum dry densities and optimum moisture contents of SSCSM. The cylinder samples with dimensions of φ150×150 mm were prepared by the compressive testing machine (Jianyi TYE-3000, China) to test the unconfined compressive strength (UCS), indirect tensile strength and compressive modulus, the beam samples with dimensions of 100×100×400 mm were prepared to test bending strength and drying shrinkage. All samples were wrapped in plastic bags and placed at the relative humidity of 95 % and the temperature of 20°C. The samples were cured for different periods according to test requirements, and for every test, a minimum of 4 samples were prepared.

2.3. Test methods

2.3.1. Hydration heat test

The hydration kinetics of SSP-cement-limestone slurry were measured by isothermal calorimeter (Lrel TAM Air, China). Before the

Table 1
Physical properties of cement.

Physical properties		Measured values
Specific surface area (kg/m^3)		372
Normal consistency (%)		27
Setting time (min)	Initial set	218
	Final set	293
3d compressive strength (MPa)		5.8
3d flexural strength (MPa)		2.71

Table 2
Physical properties of limestone aggregates.

Physical properties		Measured values
Apparent density(g/cm^3)	0–4.75 mm	2.734
	4.75–9.5 mm	2.727
	9.5–19 mm	2.729
	19–37.5 mm	2.731
Crushing value (%)		21.7
Elongated and flaky particles content (%)		1.9
Water absorption (%)		0.37

test, the calorimeter was equilibrated at 25°C for 12 h. During the preparation of the slurry, cement and SSP were first mixed according to the designed proportions in Table 4. Then, 5 g of this mixture was blended with 5 g of fine limestone aggregate, and finally, it was stirred evenly with 4 g of deionized water and sealed in the calorimeter. The change of hydration heat within 72 h was recorded.

2.3.2. Microstructure analysis

Mirco-morphology of hydration products was studied by observing the fracture surface of SSCSM under SEM (Zeiss Gemini 300, Ger). The chemical elements composition of the polymerization and hydration products were tested by using EDS analysis. Before the test, the cylinder sample was broken, and the center part was selected and coated with a layer of gold to improve the quality of images.

2.3.3. Mechanical properties

The mechanical properties of cylinder samples were investigated by UCS (at 3d, 7d, 14d, 28d), bending strength (7d), indirect tensile strength (28d) and compressive modulus (28d) of SSCSM, following the Chinese standard JTG E51–2009. The samples were soaked in water at 20°C for 24 h prior to all these tests.

2.3.4. Drying shrinkage test

Drying shrinkage will lead to cracks in CSM. The crack resistance of SSCSM was investigated by the drying shrinkage test using the beam

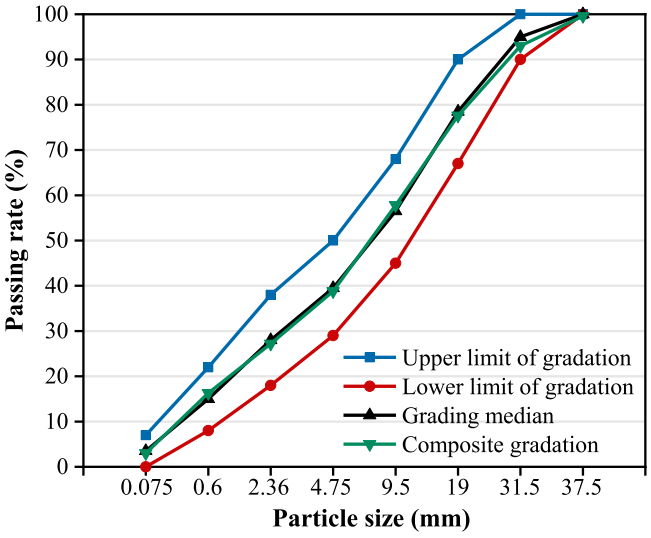

Fig. 2. Grading curves of mixture.

Table 4
Constituent proportions of cementitious material.

Samples	Gradation	Cement contents (% by weight of aggregates)	Steel slag contents (% by weight of aggregates)	Replacement level of cement (%)
SS−0	C-A−1	5	0	0
SS−10		4.5	0.5	10
SS−20		4	1	20
SS−30		3.5	1.5	30
SS−40		3	2	40

Table 3
Chemical compositions of steel slag tested with XRF.

Oxide type	CaO	Fe_2O_3	SiO_2	Al_2O_3	MgO	MnO	P_2O_5	TiO_2	SO_3	Na_2O
Oxide content (%)	35.10	21.49	19.74	7.13	6.77	3.62	1.50	1.03	0.97	0.81

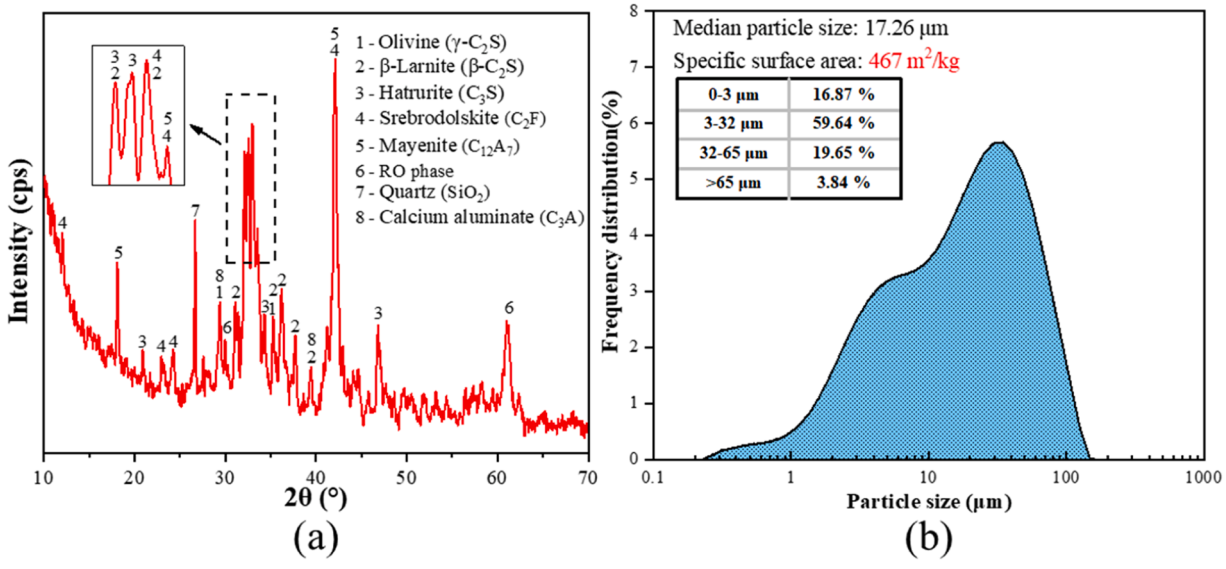

Fig. 1. XRD patterns particle size distribution of SSP, (a) XRD patterns, (b) Particle size distribution.

samples cured for 7d. The test process followed the Chinese standard JTG E51–2009. The samples were placed in an environment with the temperature of 20°C and the relative humidity of 60 %. The water loss rate of samples was recorded during the drying process. The water loss rate and drying shrinkage coefficient was determined by the following equations:

$$W_i = \frac{m_i - m_{i+1}}{m_p} \quad (1)$$

$$\alpha_d = \frac{\sum \delta_i / l}{\sum w_i} \quad (2)$$

Where i is the number of days ($1 \leq i \leq 12$); W_i is the water loss rate of the sample at i day (%); m_i and m_{i+1} are the weight of the sample at i day and i+1 day (g); m_p is the weight of the sample after drying (g); α_d is drying shrinkage coefficient (%); δ_i is the shrinkage value of the sample at i day (%); l is the length of the sample (mm).

2.3.5. Dry-wet cycling test

The dry-wet cycling test was carried out to evaluate the water damage resistance of SSCSM, following a 74h-cycling program developed by Peng et al.[35]: i) Firstly, the SSCSM samples cured for 28d were placed in an oven at 60±5°C for 48 h. ii) Subsequently, the SSCSM samples were taken out for 2 h to be cooled to ambient temperature (around 23°C), and then placed in a constant temperature water tank at 20±5°C for 24 h to complete a dry-wet cycle. iii) Finally, the dry-wet cycling test program was finished after five dry-wet cycles and the UCS test was employed to investigate the UCS of SSCSM samples after dry-wet cycles. The water stability coefficient was calculated using the following equations[36] :

$$K_r = \frac{U_{after}}{U_{before}} \quad (3)$$

Where K_r is the water stability coefficient; U_{after} is the UCS of SSCSM samples after dry-wet cycles (MPa); U_{before} is the 28d UCS of SSCSM samples (MPa).

The X-ray computed tomography (X-CT, Zeiss Xradia 510 Versa, GER) was employed to investigate the pore structure and pore distribution. The cylinder samples cured for 28d were cut into cubes with the dimensions of 40×40×40 mm. The three-dimensional pore structure before and after dry-wet cycles was detected.

2.3.6. Heavy metal ions leaching test

According to Chinese standard HJ/T 299–2007 [37], the leaching behavior of heavy metal ions in SSP under a weak acid environment such as acid rain was evaluated. Most of the acid rain in China is sulfate acid rain, so sulfuric acid and nitric acid were mixed at the weight ratio of 2:1 and then diluted with deionized water to prepare the leaching solutions with a pH of 3.20±0.05. 150 g SSP and 1500 g leaching solution were mixed evenly in the extraction bottle and sealed. The extraction bottle was fixed on the overturning oscillation device and rotated at 30 ±2 r/min for 20 h under 23±2°C. The leachate was filtered, and then 20 g of liquid was collected to measure the content of heavy metal ions (Fe, Mn, Zn, Cr, Zn) by inductively coupled plasma mass spectrometry (ICP-MS, Thermo Fisher iCAP RQ, US).

It should be noted that the standard leaching test method may not accurately assess the heavy metal leaching behavior of SSP in CSM. The SSP in SSCSM is often surrounded by hydration products and the mixture, moreover, the weight ratio of rainfall to base course is much higher than the liquid-solid ratio in traditional leaching tests, which can largely affect the leaching behavior.

Aimed to simulate the leaching behavior of SSCSM during service, a column leaching test setup for SSCSM was developed which is shown in Fig. 3. The setup is primarily consisting of a peristaltic pump and an infiltration container. The infiltration container is a cylindrical container with an inner diameter of 150 mm and a height of 300 mm, with three outlets of different heights. The leaching process is divided into three parts: i) The leaching solutions were pumped to the bottom of the infiltration container by the peristaltic pump and rose slowly. ii) When the leaching solutions gradually submerged the entire cylinder sample, it flowed out from the outlet. iii) After the leaching was completed, the leachate was centrifuged at 1500 r/min for 20 min, and then 20 g of supernatant was taken for ICP-MS test to measure the content of heavy metal ions (Fe, Mn, Zn, Cr, Zn). In order to simulate the rainfall in the natural environment, the liquid-solid ratio of leaching solutions and sample, and the flow rate of the peristaltic pump were calculated using the following equations:

$$M_w : M_s = \frac{P * \rho_a}{10} : H_s * \rho_s \# \quad (4)$$

$$S = \frac{I_R * \pi R^2}{2400} \# \quad (5)$$

Where M_w is the weight of the leaching solutions (g); M_S is the weight of the sample (g); P is the average rainfall of Hubei Province in 2022 (mm),

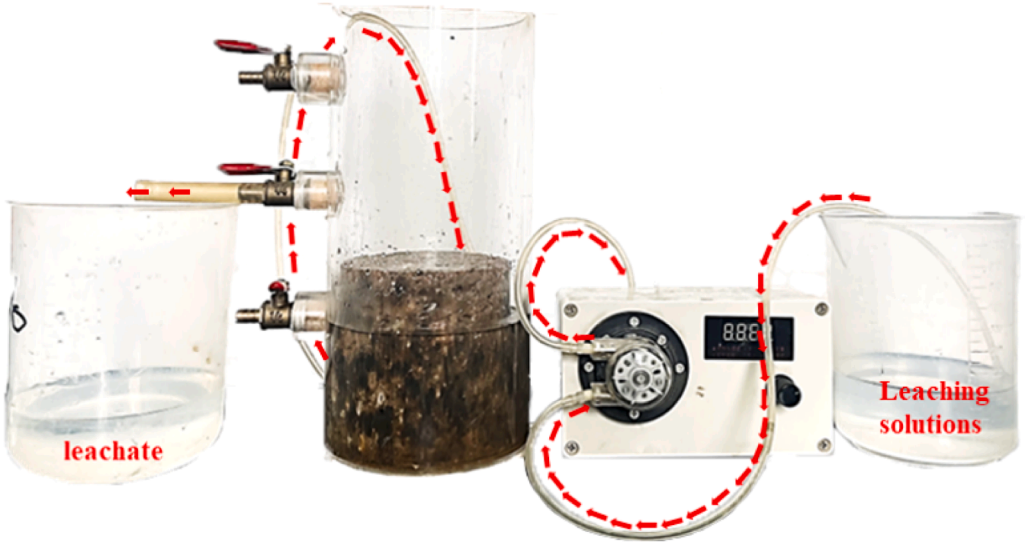

Fig. 3. Column leaching test setup.

which is 984.5 mm according to the statistics from Hubei Provincial Meteorological Bureau; ρ_a is the density of the leaching solutions (g/cm^3), which is 1 g/cm^3; H_s is the height of CSM base course in the project (cm), which is generally 20 cm; ρ_s is the dry density of the sample (g/cm^3), depending on the results of the compaction test; S is the flow rate of the peristaltic pump (ml/min); I_R is the rainfall intensity (mm/h), which is set as 10 mm/h; and R is the diameter of the infiltration container (cm).

2.3.7. Economic& environmental benefits analysis

Taking the construction of a 1 km long, 20 cm thick, and 20 m wide highway base course as an example, a cost comparison was conducted between CSM and SSCSM to evaluate the economic benefits of SSCSM. To assess the environmental benefits of CSM and SSCSM, Table 5 summarizes the energy consumption information for the manufacturing of cement, limestone, and SSP. The electricity and diesel consumption for the production of cement and limestone were obtained from the study of Anastasiou et al. [38]. As a type of solid waste, steel slag is recycled, so its energy consumption can be regarded as zero. However, the production of SSP requires ball milling of steel slag, resulting in energy consumption. The energy consumption of SSP production is calculated according to the following equation:

$$E_S = \frac{3.6 * 10^6 W_S}{M_S * 10^6} \tag{6}$$

Where E_S is the electricity consumed to produce 1 kg SSP (MJ/kg), WS is the power of the ball mill (kWh), which is set to 250kWh, and Ms is the output of the ball mill (t/h), which is set to 10t/h.

The transportation distance of materials in the life cycle of this paper is set based on the distribution of building resources in Hubei Province, China. Usually, limestone aggregates and cement can be obtained from nearby quarries and construction sites, so the transport distance of limestone aggregates is set to 50 km and that of cement is set to 20 km. However, considering that steel slag is supplied by fixed steel mills, its transport distance is longer. Therefore, the transport distance of steel slag is set to 100 km, which is a fair long distance. The IPCC 2013 GWP method developed by the Intergovernmental Panel on Climate Change was selected to calculate the environmental impact. SimaPro was used for Life cycle assessment, 1 kg mixture was used as the unit for environmental impact calculation.

3. Results and discussions

3.1. Density and moisture content of SSCSM

Compaction test was conducted on mixtures with different SSP content to investigate the effect of SSP content on the moisture content and dry density of base materials. The relationships of dry density and moisture content are shown in Fig. 4. As SSP content increased, the maximum dry densities of the mixture decreased from 2.428 g/cm^3 to 2.41 g/cm^3, and the optimum moisture contents also decreased slightly. Because SSP has a greater specific surface area and density than cement, when the weight of cementitious material is the same, with the increase of SSP substitution, the porosity of the mixture also increases, resulting in a decrease in dry density. In addition, due to the poor water absorption of SSP compared with cement, the optimum moisture content decreased with the addition of SSP.

Table 5
Energy consumption of raw materials.

Materials	Electricity (MJ/kg)	Diesel (MJ/kg)
Cement	0.36	-
Limestone	0.00828	0.000542
SSP	0.09	-

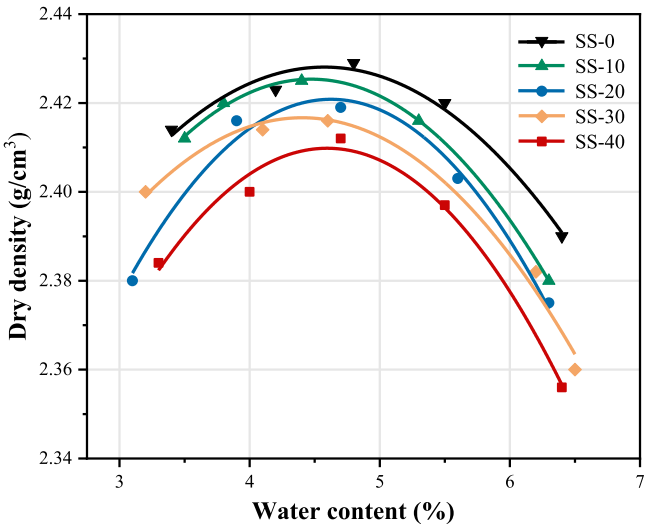

Fig. 4. Relationship of the maximum dry densities and optimum moisture contents.

3.2. Microstructure and hydration products of SSCSM

3.2.1. Hydration heat analysis

The SSP-cement-limestone mixtures' 72 h hydration heat was tested to assess the influence of SSP on the cementitious system's hydration process. Fig. 5 shows the hydration heat of the mixtures with different SSP content. The composite paste's second exothermic peak moved to the left side as SSP content increased, and the composite paste's cumulative hydration heat was reduced by the addition of SSP.

There are fewer hydralic mineral components (such as C_2S and C_3S) in steel slag than cement, and the RO phase in steel slag does not have hydration activity. In principle, SSP will reduce the amount of reactive phase in the system, making the induction period of hydration longer and the cumulative hydration heat reduced[39,40]. However, with the addition of limestone particles, It can be observed that the hydration heat showed an opposite trend, in which the induction period of mixtures decreased as SSP content rose. It might be because the limestone particles can provide nucleation sites, thereby accelerating the cement hydration kinetics, shortening the induction period, and accelerating the initial hydration process, which was supported by the findings from Ye et al. [41]. Similar to limestone particles, some studies have also reported the nucleation effect of SSP [42,43]. Therefore, with the incorporation of SSP, the mixtures' early hydration process is promoted, so the second exothermic peak appears in advance, but the total amount of hydration products reduced.

3.2.2. Micro-morphology examination on the hydrated mixture

The micro-morphology of SS-0 and SS-40 are shown in Fig. 6. It is evident that SS-0's structure is denser than SS-40, and the limestone aggregates in SS-0 are combined into a uniform whole through hydration products, while the structure of SS-40 is looser. This might be attributed to two factors. Firstly, as discussed in Section 3.1 of this paper, the particle characteristics of SSP lead to more pores and defects in SS-40. Secondly, the nucleation effect of SSP makes the SSP in the mixture become the site of hydration, and the disparity in hydration rates between SSP and cement results in an uneven distribution of hydration products.

Fig. 7 shows the SEM images of hydration products distribution for SS-0 and SS-40. It can be observed that the flocculent hydration product is widely distributed inside SS-0 and SS-40. The EDS results show that the primary chemical elements of the flocculent product are Ca, Si and O, indicating that it is flocculent C-S-H gel. In Fig. 7(b), the needle-like hydration product can be clearly observed. EDS results show that the

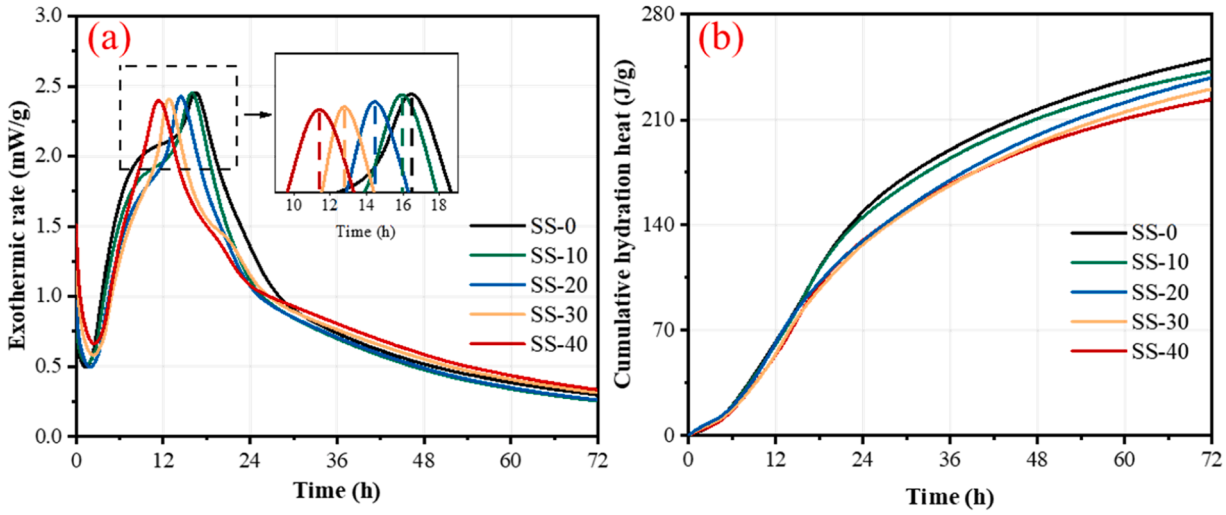

Fig. 5. Calorimetry curves of composite paste, (a) Heat flow, (b) Cumulative heat.

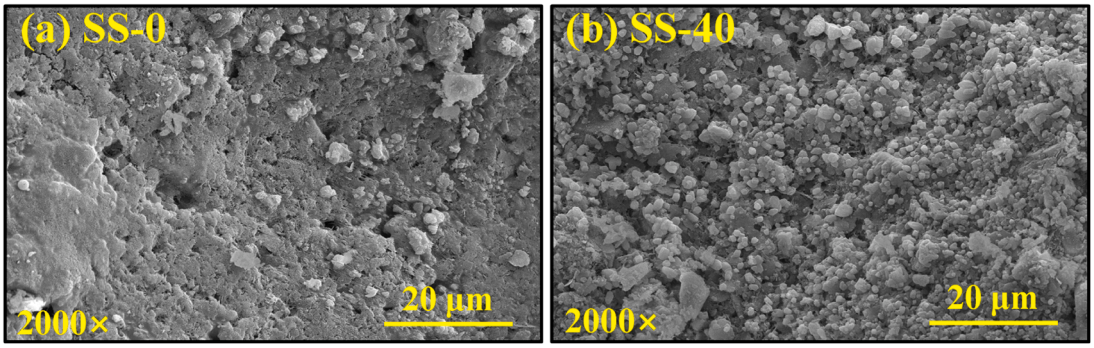

Fig. 6. SEM images of cylinder samples with different SSP content, (a) SS-0 magnified by 2000 times, (b) SS-40 magnified by 2000 times.

primary chemical elements of the needle-like product are Ca, Si, O and S, indicating that it is needle-like ettringite (AFt) crystals. C-S-H is produced by the reaction of β-C_2S and C_3S with H_2O. AFt is produced by the reaction of C_3A with $CaSO_4$ and H_2O. The hydration reaction of C-S-H and AFt can be approximated as:

$$2\,(3CaO{\blacksquare}SiO_2 + 6H_2O) \rightarrow CaO{\blacksquare}2SiO_2{\blacksquare}3H_2O + 3Ca(OH)_2 \quad (7)$$

$$3CaO{\blacksquare}Al_2O_3 + 3CaSO_4{\blacksquare}2H_2O + 26H_2O \rightarrow 3CaO{\blacksquare}Al_2O_3{\blacksquare}3CaSO_4{\blacksquare}32H_2O \quad (8)$$

C-S-H and AFt play the main role of bonding aggregates, and strengthen the mechanical properties of SSCSM. Fig. 7(a) shows that the C-S-H gel covers the surface of the aggregate, filling the gap between SSCSM samples and connecting aggregates. However, as shown in Fig. 7 (b), the C-S-H gel on the surface of SS-40 is less than that of SS-0, which might be because the content of calcium silicate (C_2S and C_3S) in cement is more than that in steel slag, SS-40 produces fewer hydration products than SS-0. The hydration heat results also confirmed the decrease of hydration products with the incorporation of SSP. Therefore, with the increase of SSP, the C-S-H gel formed by hydration is not enough to form a stable hydration network, and the pores in the mixture increase. In addition, as shown in Fig. 7(b), AFt crystals fill the gap of the C-S-H, providing support for the mixture's strength. AFt crystals will also produce crystallization stress inside the mixture. When the sample is dried, the crystallization stress can counteract the capillary tension caused by water loss and enhance the mixture's shrinkage performance [44].

3.3. Performance of SSCSM

3.3.1. Mechanical property

The base course of an asphalt pavement serves as the primary load-bearing layer, therefore, the UCS is an important parameter for CSM. According to the Chinese standard JTG/T F20–2015, CSM needs to have a minimum 4 MPa 7d UCS for serving as the base course. Fig. 8 presents the 3d, 7d, 14d and 28d UCS of SSCSM samples with different SSP content. It shows that the UCS decreases with the incorporation of SSP, and for the samples with the same SSP content, as the duration of curing time increases, the UCS increases. The UCS of the samples at 7d from high to low is SS-0 (5.1 MPa), SS-10 (4.7 MPa), SS-20 (4.5 MPa), SS-30 (4.2 MPa) and SS-40 (3.9 MPa). The UCS of the samples reaches 4 MPa when the content of SSP does not exceed 30 %, which satisfies the requirement for engineering application.

The strength and stiffness of SSCSM are shown in Fig. 9. The bending strength, indirect tensile strength and compressive modulus of SSCSM samples decrease with the increase of SSP content, which follows the same trend as UCS. It might be because cementitious mineral components such as C_2S and C_3S in steel slag are less reactive, so the addition of SSP resulted in a decrease of hydration products. This is demonstrated by the hydration heat results presented in Section 3.2.1 of this paper. The reduction of C-S-H gel reduced the structural stability of SSCSM samples, thus reducing the strength and stiffness of the SSCSM samples. The high porosity of SSCSM also has an unfavorable influence on the UCS. The structural uniformity of SSCSM samples will be impacted by the increase of pore size, making it more prone to stress concentration when stressed, resulting in the decrease of strength.

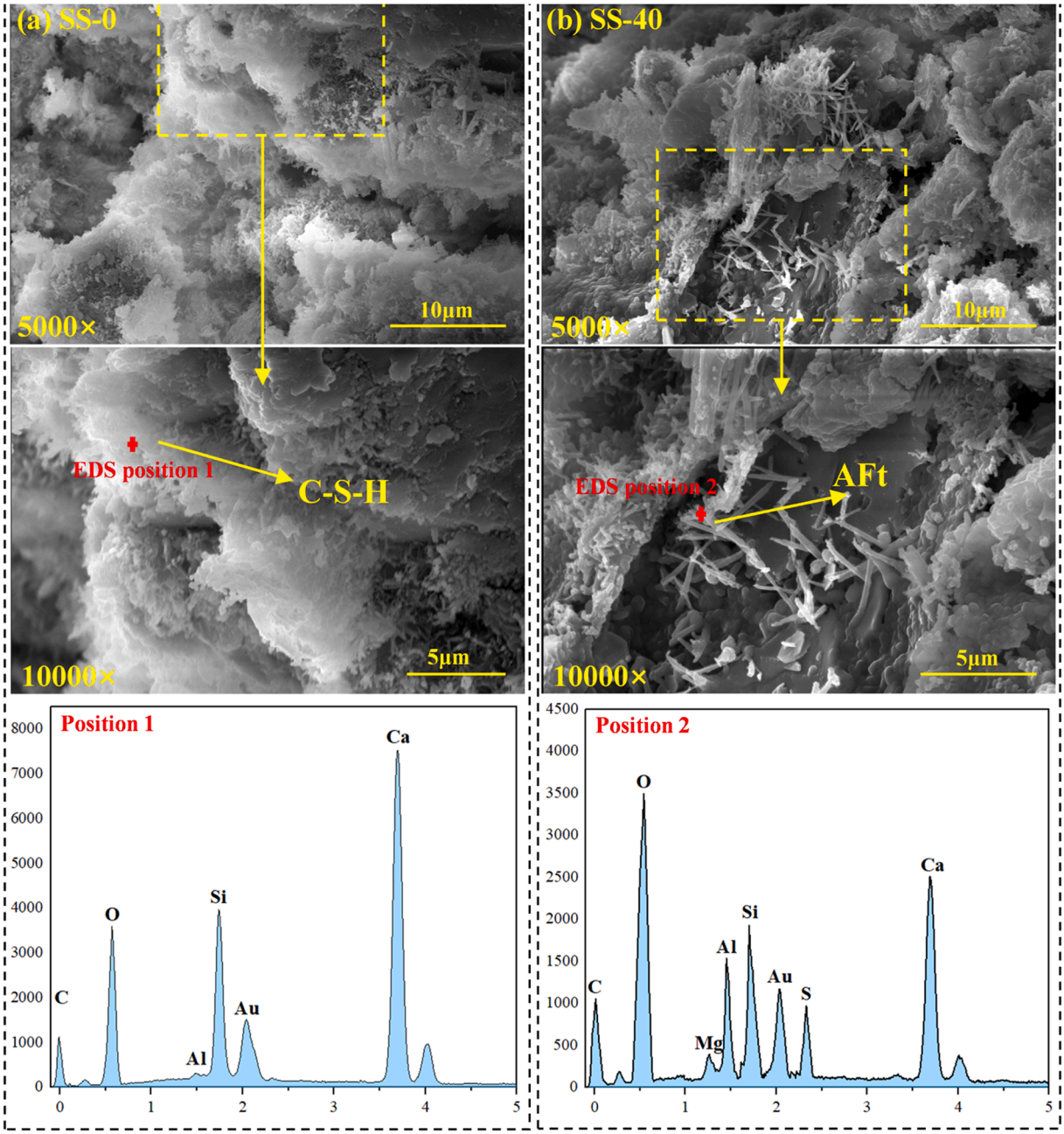

Fig. 7. SEM images and EDS results of hydration products, (a) SS-0, (b) SS-40.

3.3.2. *Shrinkage performance*

The drying shrinkage coefficient and water loss rate of beam samples are affected by the incorporation of SSP, as shown in Fig. 10. It is evident that after 12d, the beam sample's drying shrinkage and water loss tended to remain stable, and as SSP content increased, the water loss rate of the beam samples increased and the drying shrinkage coefficient decreased. With SSP content rose from 0 % to 40 %, the beam samples' water loss rate at 12d increased from 2.8 % to 4.4 %. Compared with the beam samples without SSP, the drying shrinkage coefficient of the beam samples with 40 % SSP at 12d decreased by 32 %, demonstrating that the addition of SSP limits the drying shrinkage of SSCSM samples therefore shows higher resistance to drying shrinkage.

SSP hydrates more slowly than cement during the early stages. As the SSP content increased, the amount of chemically bonded water in SSCSM samples decreased, and more free water led to the increase of water loss rate of SSCSM samples. However, Steel slag contains f-CaO, which can produce $Ca(OH)_2$ when it reacted with water, causing volume expansion[32]. In asphalt concrete, when using steel slag as aggregates, its volume expansion will destroy the structure of pavement[45]. In SSCSM, the volume expansion of SSP may partially counteract the drying shrinkage, leading to a reduction in the shrinkage value, so the drying shrinkage coefficient of SSCSM samples reduced as SSP content increased.

3.3.3. *Water damage resistance*

Table 6 summarizes the UCS of cylinder samples before and after dry-wet cycles and the water stability coefficient of samples. The findings show that when SSP content increased, the samples' water stability coefficient reduced. After dry-wet cycles, the UCS of SS-0 dropped from 7.22 MPa to 6.24 MPa, and the K_r was 0.865. When SSP content reached 40 %, the UCS of SS-40 decreased from 4.97 MPa to 3.67 MPa, and the K_r of the sample was 0.738. The addition of SSP reduced the water

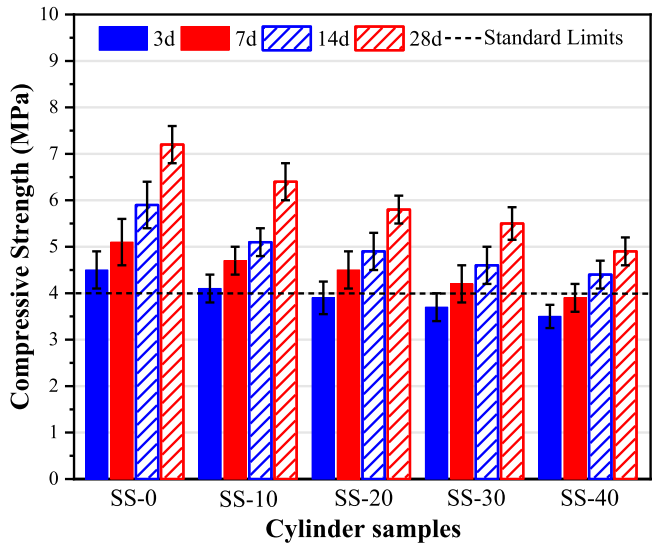

Fig. 8. Results of unconfined compression strength at 3d, 7d, 14d and 28d.

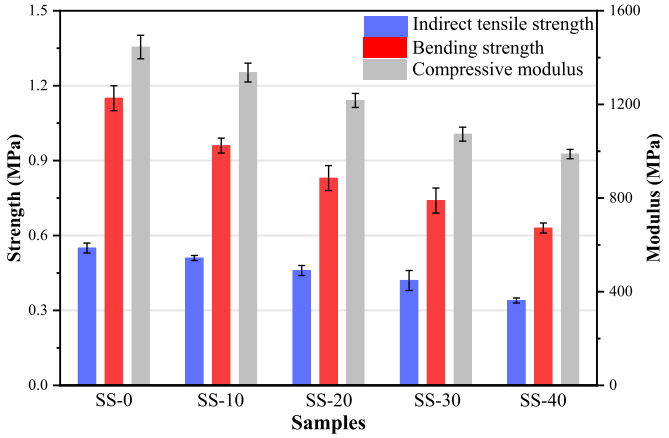

Fig. 9. The results of the indirect tensile strength, bending strength and compressive modulus of the SSCSM samples at 28d.

damage resistance of the samples. But all samples' K_r are greater than 0.7, which satisfies the engineering application's requirements for durability [36].

Fig. 11 shows the CT results of the SSCSM samples before and after dry-wet cycles, and the impact of water damage on the structure of SSCSM samples can be observed clearly. After dry-wet cycles, SS-0's porosity rose from 1.58 % to 2.37 %, and SS-40's porosity increased from 2.03 % to 3.16 %. The connected layered pores in the samples are caused by the breakage of limestone aggregates during compaction; The unconnected pores represent the voids inside the sample that are not filled by aggregates and hydration products. It can be observed that SS-40 has more non-connected pores than SS-0, which indicates that the internal structure of the SSCSM sample becomes looser with the addition of SSP, thereby increasing the SSCSM sample's water penetration. The porosity of SS-40 increased by 1.13 % after dry-wet cycles, which was much higher than that of SS-0 (0.79 %), demonstrating that the addition of SSP not only increased the sample's initial porosity, but also increased the porosity of the sample after water damage. After the dry-wet cycles, the sample's porosity increased, increasing the probability of stress concentration when the sample was strained, thereby reducing the UCS of the sample.

To further discuss the pore size distribution of SSCSM before and after the dry-wet cycles, a fitting was done for the pore size distribution. The following equation displays the probability function [46]:

$$f(D) = \frac{1}{\sigma\sqrt{2\pi}}\exp^{\left(-\frac{(D-\mu)}{2\sigma^2}\right)}\# \quad (9)$$

Where $f(D)$ and D are probability function and pores diameter, respectively. σ is the standard deviation. Fig. 12 depicts the pores' diameter distribution and normal distribution fitting curves. It can be seen that after the dry-wet cycles, the average pore diameter of SS-0 increased from 65.2μm to 72.5μm, and the standard deviation(σ) increased from 24.3 to 27.1. The average pore diameter of SS-40 increased from 66.4μm to 78.1μm, and the standard deviation(σ) increased from 22.0 to 29.2.

Table 6
Results of dry-wet cycling test and Kr of samples with different SSP content.

Samples	U_{after} (MPa)	U_{before} (MPa)	K_r
SS−0	7.22	6.24	0.865
SS−10	6.45	5.42	0.841
SS−20	5.83	4.74	0.813
SS−30	5.51	4.28	0.776
SS−40	4.97	3.67	0.738

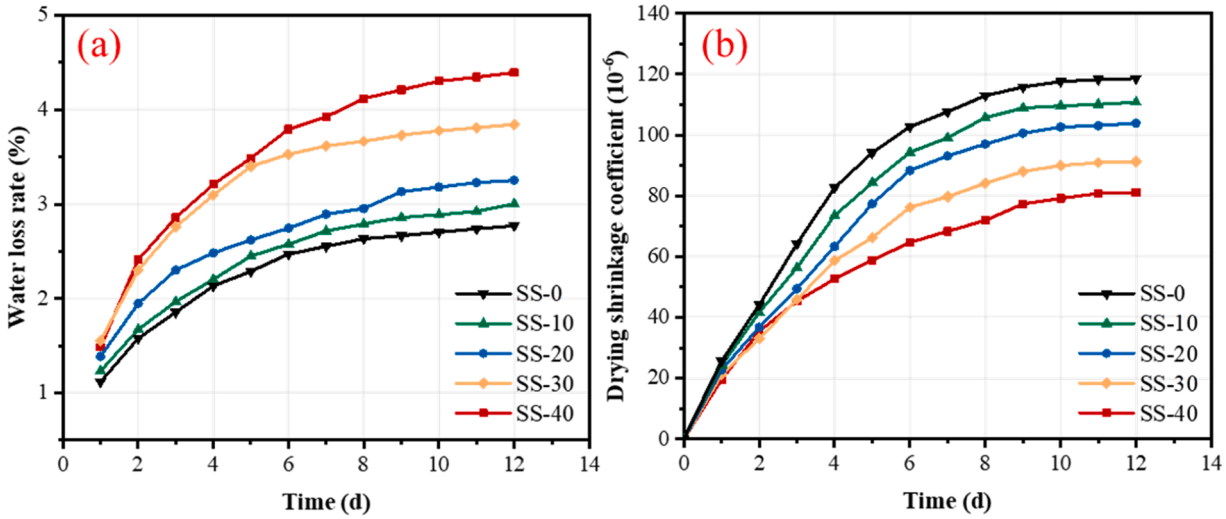

Fig. 10. Shrinkage development of SSCSM samples with different SSP contents, (a) Water loss rate; (b) Drying shrinkage coefficient.

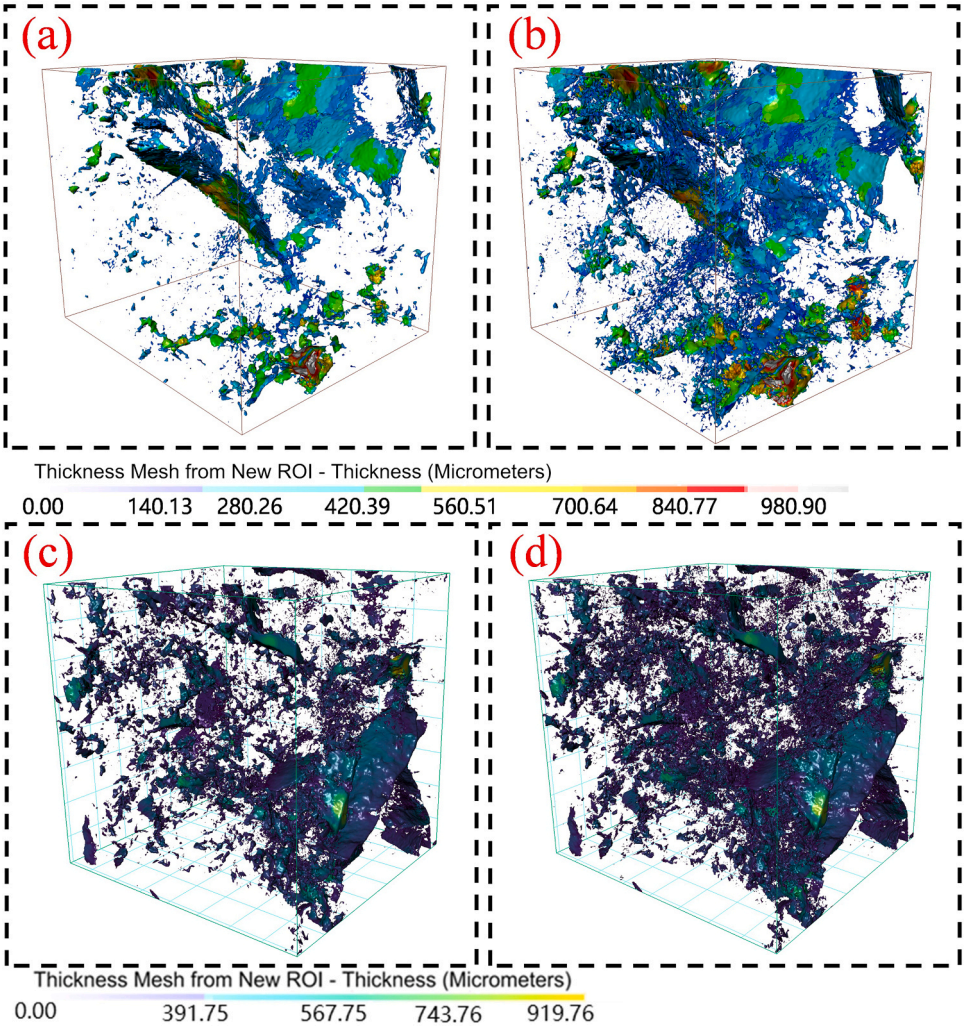

Fig. 11. Three-dimensional pores of samples with different SSP contents, (a) SS-0 before dry-wet cycles, (b) SS-0 after dry-wet cycles, (c) SS-40 before dry-wet cycles, (b) SS-40 after dry-wet cycles.

The findings showed that the average pore diameter and standard deviation of SSCSM both increased after water immersion, and the diameter and standard deviation increased more significantly after the additon of SSP. The increase of standard deviation means that the pore size distribution becomes larger. This indicated that after the dry-wet cycles, not only new pores were generated inside the sample [47], but also the original pores will expand or even connect with each other. Hence, the addition of SSP not only increased the initial porosity of SSCSM, but also promoted the development of pores in SSCSM samples after water immersion.

The above findings indicate that the incorporation of SSP deteriorates the strength and the water stability of SSCSM through the following three different ways:

(1) Considering SSP's high specific surface area and density, the addition of SSP increased the initial porosity of SSCSM samples and accelerated the penetration of water. Consequently, the capillary tension of water inside the SSCSM samples increased.
(2) The incorporation of SSP decreased the amount of hydration products and weakened the connection of C-S-H, which made it hard to form a stable hydration network. Therefore, compared with CSM, the repeated infiltration of water in SSCSM will destroy the hydration structure of the mixtures and reduce the stability of SSCSM samples.
(3) When water penetrated into SSCSM, the SSCSM samples' internal structure was destroyed as a result of the high capillary tension inside the sample and the loose structure of the hydration products. The average pore diameter of the sample increased and the pore size distribution became larger, it leads to the increase of porosity and connected pores in the SSCSM samples. Consequently, the SSCSM sample was more prone to stress concentration, showing a decrease of UCS and water stability coefficient.

3.4. Environmental feasibility

3.4.1. Heavy metal ions leaching behavior of SSP

The leaching concentration of heavy metal ions for SSP is shown in Table 7. The leaching concentration of Fe in SSP was the highest (19.78 mg/L), because steel slag contains a lot of iron oxide, which will react with acidic leaching solutions. The leaching concentration of Cr was the lowest, only 0.024 g/ml. The content of MnO in steel slag was less than that of FeO, but the leaching concentration of Mn in SSP (17.52 mg/L) was close to that of Fe. This is because the reactivity of Mn with acid is higher than that of Fe, which will make more Mn dissolve in the leaching solutions. The Chinese standard GB/T 14848–2017's Class IV water requirements [48] are exceeded by the leaching concentrations of Fe, Mn, Zn, and Pb in the leaching solutions of SSP, demonstrating that the concentration of heavy metal ions in the SSP leaching solutions is too high to be utilized as drinking water. The accumulated steel slag

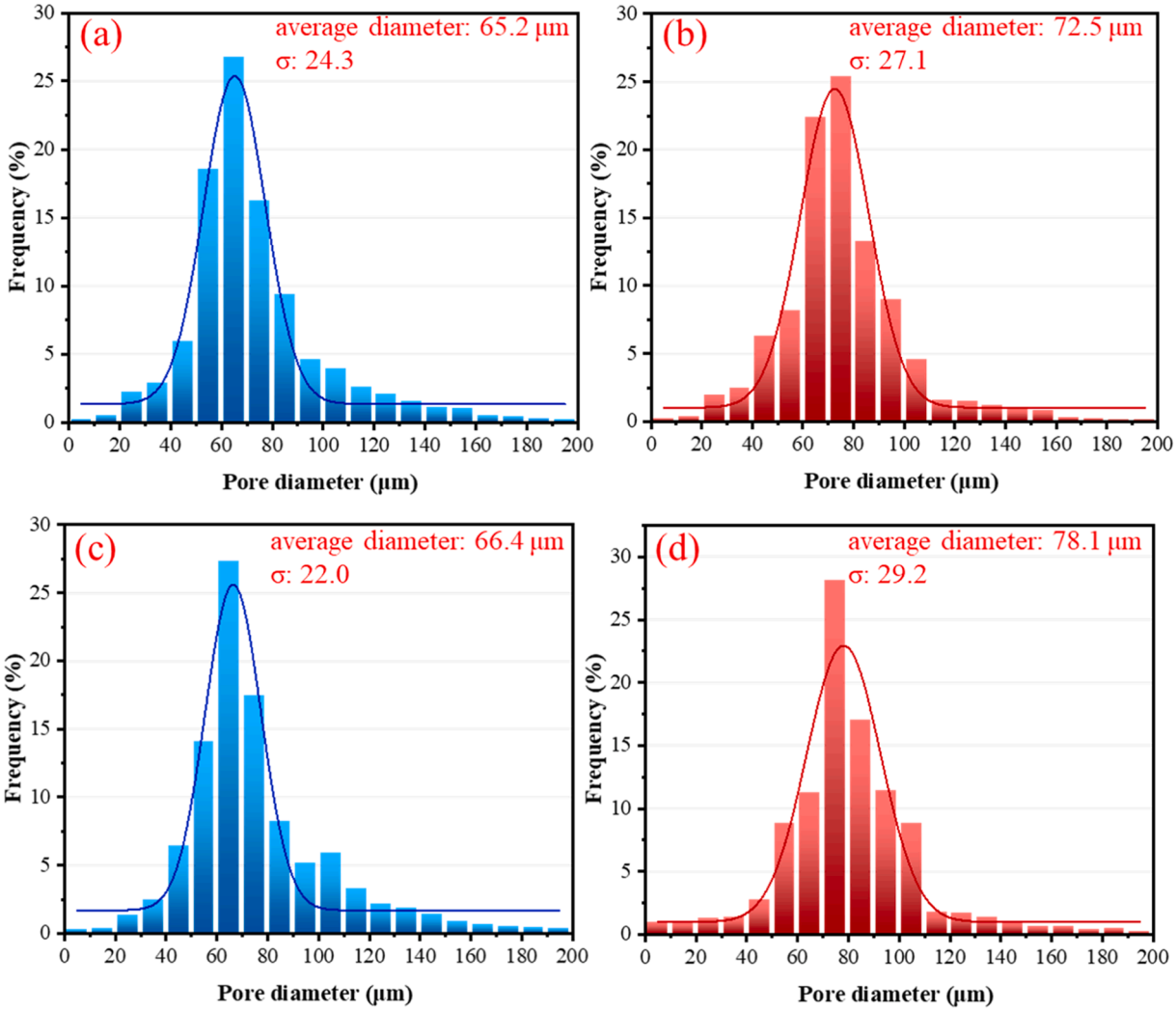

Fig. 12. Pore size distribution of SSCSM, (a) SS-0 before dry-wet cycles, (b) SS-0 after dry-wet cycles, (c) SS-40 before dry-wet cycles, (d) SS-40 after dry-wet cycles.

Table 7
The heavy metal ions leaching concentration value of SSP.

Heavy metal ions		SSP	Standard Limits (GB/T 14848–2017)
Leaching concentration (mg/L)	Fe	19.78	<2
	Mn	17.52	<1.5
	Zn	8.72	<5
	Cr	0.024	<0.1
	Pb	1.28	<0.1

will leach a significant amount of heavy metal ions after contact with water, leading to significant soil and water pollution in the environment.

3.4.2. *Heavy metal ions leaching behavior of SSCSM*

Fig. 13 shows the column leaching test results for SSCSM samples. The amounts of heavy metal ions leaching from SSCSM increased as the SSP content rose, however, compared to SSP, all SSCSM samples' leaching concentrations were substantially lower. In SSCSM, the SSP is covered by hydration products which form a protection barrier that prevented the RO phase (FeO and MnO) in the steel slag from coming into contact with the acidic leaching solutions. As a result, the leaching concentrations of Fe and Mn were significantly reduced. Compared with SSP, the concentration of Fe and Mn in the leaching solutions of SS-40 decreased by 92.2 % and 99.9 %, respectively, while Zn, Cr, and Pb leaching concentrations also dropped by 44.9 %, 61.7 % and 90.7 %. In all SSCSM samples, only the leaching concentration of Pb in SS-40 was higher than the standard limits. Therefore, when the content of SSP is less than 30 %, the leaching concentrations of heavy metal ions in SSCSM are relatively low, and the leaching solutions can meet the requirements of Class IV water in China, which can be used as domestic water for residents after treatment.

3.5. *Economic& environmental benefits of SSCSM*

Although there may be additional costs incurred during the grinding and transportation of SSP raw materials, the SSP accounts for only 2 % of the total weight of base course materials. Therefore, these expenses are negligible compared to the overall construction costs of SSCSM. Hence, it can be assumed that the expenses for producing CSM and SSCSM with 30 % SSP are identical since the overall transportation and production processes of SSCSM are similar to those of conventional cement-based CSM. However, as a byproduct of the metallurgical industry, the cost of steel slag is significantly less than cement. As shown in Table 8, the price of SSP is only 48 % of cement. When using SSP to replace 30 % of cement, it is expected to achieve a net economic saving of 4 % of the base course expenditure.

Fig. 14 are the equivalent CO_2 produced during the production of CSM and SSCSM. The equivalent CO_2 produced by 1 kg CSM and 1 kg SSCSM are 0.0553 kg and 0.0423 kg, respectively. The equivalent CO_2

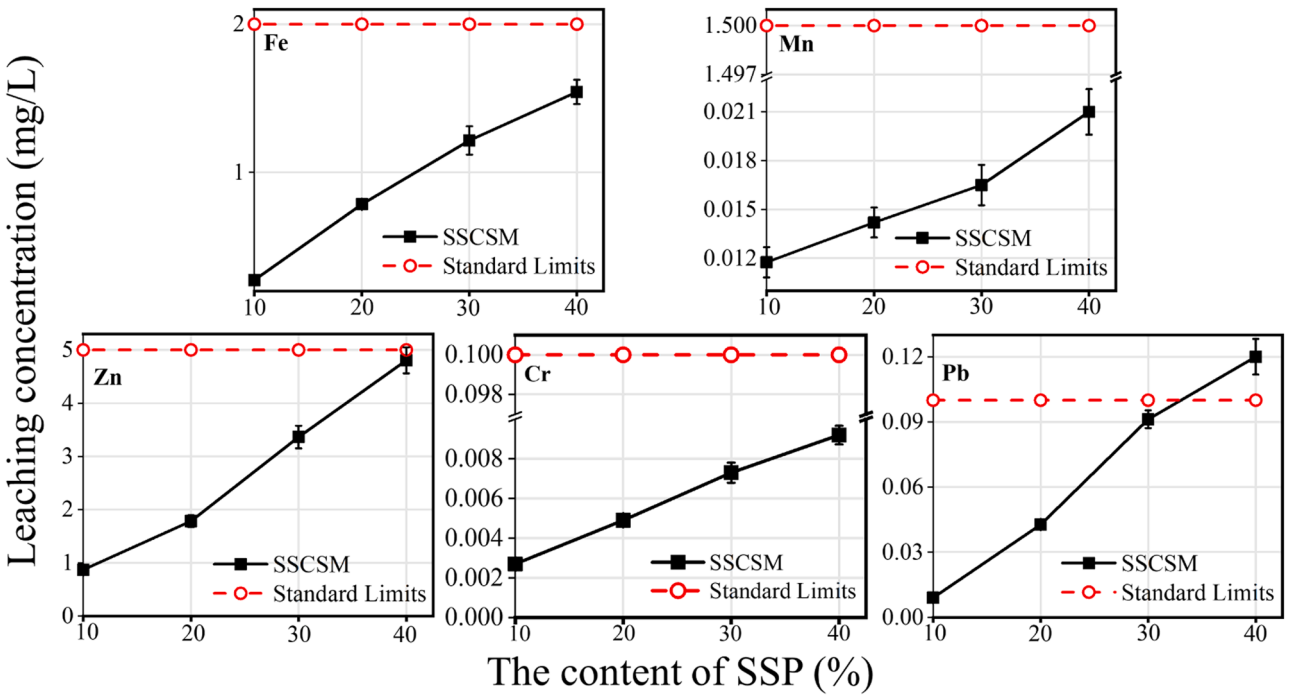

Fig. 13. The leaching concentration of heavy metal ions in samples with different content of SSP.

Table 8
Cost of raw materials.

Item		Unit (¥/t)	CSM		SSCSM with 30 % SSP	
			Amount/t	Cost/¥	Amount/t	Cost/¥
Materials	Cement	500	486	243000	337	168500
	SSP	240	-	-	145	34800
	Limestone	110	8748	962280	8676	954360
	Water	2.5	437	1093	414	1035
Total		-	-	1206373	-	1158695

Note: The unit price comes from Wuhan Construction Bureau in January 2023, China.

produced by cement is the most, accounting for 79.4 % and 65.7 % of the emissions of CSM and SSCSM, respectively, which follows the expectation. Because the cement manufacture will consume significant amounts of electricity and diesel. Therefore, using SSP to replace cement can reduce equivalent CO_2 emissions. When using SSP to replace 30 % cement to produce SSCSM, the equivalent CO_2 produced by the mixture is reduced by 23.5 %, indicating that using SSCSM as base course can produce great environmental benefits.

The use of SSCSM will reduce the cost of raw materials and significantly lower the equivalent CO_2 emissions in road engineering. In addition, as the main waste product of iron and steel industry, the use of steel slag will also save a lot of land resources and natural resources, which is helpful to achieve the clean production of road materials.

4. Conclusions

In this study, SSP was utilized to substitute the cement in CSM in different content (10 %, 20 %, 30 % and 40 % by weight). The hydration process, microstructure, mechanical properties, shrinkage properties and water damage resistance of SSCSM were investigated. Column leaching tests were conducted to simulate the leaching behavior of heavy metal ions of SSCSM, and the economic and environmental benefits of SSCSM were calculated. The following conclusions can be drawn:

(1) The maximum dry densities and optimum moisture contents of SSCSM decrease with the addition of SSP. The nucleation effect of SSP accelerates the early hydration, but the C-S-H produced by hydration is not sufficient to form a stable hydration product network, therefore, the microstructure of SSCSM is looser than that of CSM.
(2) When the content of SSP does not exceed 30 % of the total cementitious material, the strength of SSCSM meets the requirements of engineering application. The f-CaO in SSP will react with water to cause volume expansion, which can inhibit the drying shrinkage of SSCSM, therefore, its drying shrinkage performance is better than that of CSM. The water damage resistance of SSCSM is weaker than that of CSM, but its water stability still meets the durability requirements of engineering applications.
(3) In comparison to steel slag, the leaching concentration of heavy metal ions in SSCSM is substantially lower. The heavy metal ions in SSCSM with no more than 30 % substitution of SSP will not produce serious environmental pollution.
(4) SSCSM prepared by using SSP to replace 30 % cement can reduce 4 % of raw material cost and 23.5 % of equivalent CO_2 emission, which has sound economic and environmental benefits.

In conclusion, SSCSM can satisfy the application requirements of the base course and is conducive to the cleaner production of road materials. Therefore, SSCSM has good application potential in the base course of pavement.

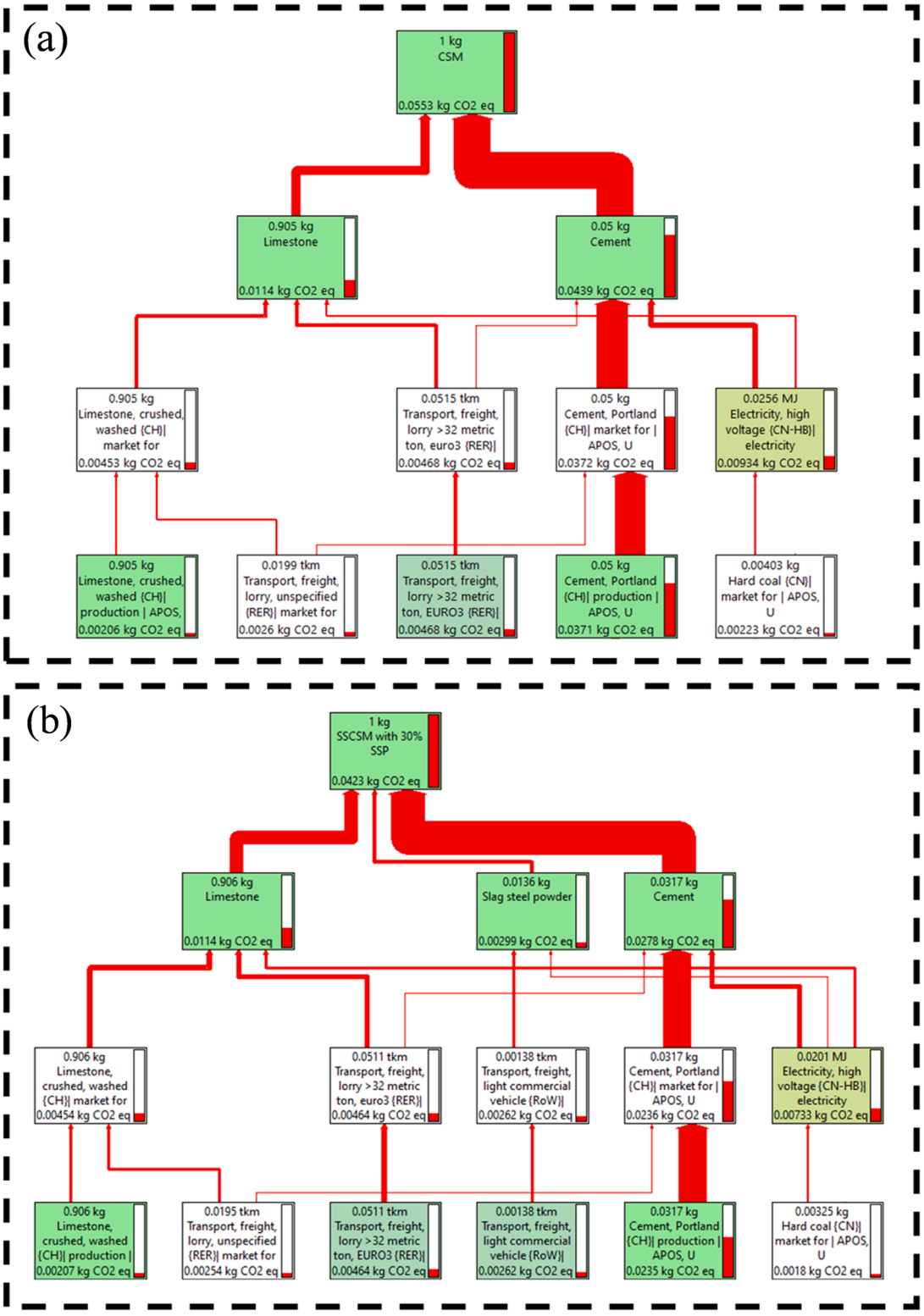

Fig. 14. CO_{2eq} emissions of CSM and SSCSM,(a) CSM, (b) SSCSM.

5. Recommendations

The steel slags have a slower hydration process compared with the conventional cement, therefore the curing time after construction should not be less than 10d to ensure the strength and reduce the water damage influence. In addition, based on the water damage process of SSCSM, it is also recommended to use Stone Mastic Asphalt (SMA) or dense graded asphalt as surface courses, and a layer of tack coat that prevents water penetrating into the SSCSM base course.

It can be considered to activate SSP by alkali activators or high-hydration activity solid waste (such as blast furnace slag) to further strengthen SSCSM's strength. Furthermore, the bond strength between SSP and aggregate lacks quantitative analysis, and the water damage resistance of SSCSM also needs to be further improved. These critical

issues will be covered in a follow-up more in-depth study.

CRediT authorship contribution statement

Xinkui Yang: Writing – original draft, Methodology, Conceptualization. **Guang Ye:** Investigation, Formal analysis. **Shi Xu:** Supervision, Project administration. **Shaopeng Wu:** Methodology, Conceptualization. **Boyu Chen:** Investigation, Formal analysis.

Declaration of Competing Interest

The authors declare that they have no known competing financial interests or personal relationships that could have appeared to influence the work reported in this paper.

Data availability

Data will be made available on request.

Acknowledgements

The project is funded by National Natural Science Foundation of China (No. 52378461), Key R&D Program of Guangxi Province (No. AB21196061), Hubei Science and Technology Innovation Talent and Service Project (No. 2022EHB006), and Science and Technology Project of the Department of Transportation of Guangxi Autonomous Region (No. 2021-MS5-125).

References

[1] Y. Zhao, P. Wu, J. Qiu, Z. Guo, Y. Tian, X. Sun, X. Gu, Recycling hazardous steel slag after thermal treatment to produce a binder for cemented paste backfill, Powder Technol. 395 (2022) 652–662.
[2] F. Bullerjahn, G. Bolte, Composition of the reactivity of engineered slags from bauxite residue and steel slag smelting and use as SCM for Portland cement, Constr. Build. Mater. 321 (2022) 126331.
[3] Z. Zhao, Z. Wang, S. Wu, J. Xie, C. Yang, N. Li, P. Cui, Road performance, VOCs emission and economic benefit evaluation of asphalt mixture by incorporating steel slag and SBS/CR composite modified asphalt, Case Stud. Constr. Mater. (2023) e01929.
[4] H. Xu, S. Wu, A. Chen, Y. Zou, C. Yang, P. Cui, Study on preparation and characterization of a functional porous ultra-thin friction course (PUFC) with recycled steel slag as aggregate, J. Clean. Prod. 380 (2022) 134983.
[5] C. Yang, S. Wu, P. Cui, S. Amirkhanian, Z. Zhao, F. Wang, L. Zhang, M. Wei, X. Zhou, J. Xie, Performance characterization and enhancement mechanism of recycled asphalt mixtures involving high RAP content and steel slag, J. Clean. Prod. 336 (2022) 130484.
[6] X. Zhao, Y. Sheng, H. Lv, H. Jia, Q. Liu, X. Ji, R. Xiong, J. Meng, Laboratory investigation on road performances of asphalt mixtures using steel slag and granite as aggregate, Constr. Build. Mater. 315 (2022) 125655.
[7] J. Liu, B. Yu, Q. Wang, Application of steel slag in cement treated aggregate base course, J. Clean. Prod. 269 (2020) 121733.
[8] J. Guo, Y. Bao, M. Wang, Steel slag in China: Treatment, recycling, and management, Waste Manag. 78 (2018) 318–330.
[9] J. Wang, M. Zhong, P. Wu, S. Wen, L. Huang, P. Ning, A review of the application of steel slag in CO2 fixation, ChemBioEng Rev. (2021).
[10] N. Shao, S. Li, F. Yan, Y. Su, F. Liu, Z. Zhang, An all-in-one strategy for the adsorption of heavy metal ions and photodegradation of organic pollutants using steel slag-derived calcium silicate hydrate, J. Hazard. Mater. 382 (2020) 121120.
[11] X. Shi, X. Wang, X. Wang, Dual waste utilization in cemented paste backfill using steel slag and mine tailings and the heavy metals immobilization effects, Powder Technol. 403 (2022) 117413.
[12] Q. Liu, J. Li, Z. Lu, X. Li, J. Jiang, Y. Niu, Y. Xiang, Silicomanganese slag: Hydration mechanism and leaching behavior of heavy metal ions, Constr. Build. Mater. 326 (2022) 126857.
[13] Y. Rui, C. Qian, CO2-fixing steel slag on hydration characteristics of cement-based materials, Constr. Build. Mater. 354 (2022) 129193.
[14] H. Zhu, M. Ma, X. He, Z. Zheng, Y. Su, J. Yang, H. Zhao, Effect of wet-grinding steel slag on the properties of Portland cement: an activated method and rheology analysis, Constr. Build. Mater. 286 (2021) 122823.
[15] P. Liu, L. Mo, Z. Zhang, Effects of carbonation degree on the hydration reactivity of steel slag in cement-based materials, Constr. Build. Mater. 370 (2023) 130653.
[16] Y. Ma, Y. Luo, H. Ma, X. Zhou, Z. Luo, Upcycling steel slag in producing eco-efficient iron–calcium phosphate cement, J. Clean. Prod. 371 (2022) 133688.
[17] L. Pang, S. Liao, D. Wang, M. An, Influence of steel slag fineness on the hydration of cement-steel slag composite pastes, J. Build. Eng. 57 (2022) 104866.
[18] A.C.P. Martins, J.M. Franco de Carvalho, L.C.B. Costa, H.D. Andrade, T.V. de Melo, J.C.L. Ribeiro, L.G. Pedroti, R.A.F. Peixoto, Steel slags in cement-based composites: an ultimate review on characterization, applications and performance, Constr. Build. Mater. 291 (2021) 123265.
[19] O. Gencel, O. Karadag, O.H. Oren, T. Bilir, Steel slag and its applications in cement and concrete technology: a review, Constr. Build. Mater. 283 (2021) 122783.
[20] S. Zhuang, Q. Wang, Inhibition mechanisms of steel slag on the early-age hydration of cement, Cem. Concr. Res. 140 (2021) 106283.
[21] S.K. Singh, Jyoti, P. Vashistha, Development of newer composite cement through mechano-chemical activation of steel slag, Constr. Build. Mater. 268 (2021) 121147.
[22] T. Zhang, B. Ma, S. Wu, Z. Jin, J. Wang, Mechanical properties and hydration process of steel slag-cement binder containing nano-SiO2, Constr. Build. Mater. 314 (2022) 125660.
[23] J. O'Connor, T.B.T. Nguyen, T. Honeyands, B. Monaghan, D. O'Dea, J. Rinklebe, A. Vinu, S.A. Hoang, G. Singh, M.B. Kirkham, N. Bolan, Production, characterisation, utilisation, and beneficial soil application of steel slag: a review, J. Hazard. Mater. 419 (2021) 126478.
[24] J. Liu, G. Xie, Z. Wang, Z. Li, X. Fan, H. Jin, W. Zhang, F. Xing, L. Tang, Synthesis of geopolymer using municipal solid waste incineration fly ash and steel slag: hydration properties and immobilization of heavy metals, J. Environ. Manag. 341 (2023) 118053.
[25] Y. Gan, C. Li, J. Zou, W. Wang, T. Yu, Evaluation of the impact factors on the leaching risk of steel slag and its asphalt mixture, Case Stud. Constr. Mater. 16 (2022) e01067.
[26] X. Wang, K. Wang, J. Li, W. Wang, Y. Mao, S. Wu, S. Yang, Heavy metals migration during the preparation and hydration of an eco-friendly steel slag-based cementitious material, J. Clean. Prod. 329 (2021) 129715.
[27] X. Sun, J. Liu, Y. Zhao, J. Zhao, Z. Li, Y. Sun, J. Qiu, P. Zheng, Mechanical activation of steel slag to prepare supplementary cementitious materials: a comparative research based on the particle size distribution, hydration, toxicity assessment and carbon dioxide emission, J. Build. Eng. 60 (2022) 105200.
[28] S. Lv, X. Peng, J. Yuan, H. Liu, L. Hu, S. Yang, J. Liu, Stress path investigation of fatigue characteristics of cement stabilized macadam, Constr. Build. Mater. 292 (2021) 123446.
[29] X. Xia, D. Han, Y. Ma, Y. Zhao, D. Tang, Y. Chen, Experiment investigation on mix proportion optimization design of anti-cracking stone filled with cement stabilized macadam, Constr. Build. Mater. 393 (2023) 132136.
[30] S. Shi, N. Wang, C. Chen, T. Ma, F. Chen, G. Gu, Multiscale study of the effect of fly ash geopolymer on the fatigue cracking of cement stabilized macadam, Constr. Build. Mater. 369 (2023) 130464.
[31] X. Lan, X. Zhang, Z. Hao, Y. Wang, Strength and shrinkage properties of cement stabilized macadam bases incorporating 0–2.36 millimetre recycled fine aggregate, Case Stud. Constr. Mater. 16 (2022) e00984.
[32] C. Qian, H. Yi, W. Du, Bacteria fixing CO2 to enhance the volume stability of ground steel slag powder as a component of cement-based materials aiming at clean production, J. Clean. Prod. 314 (2021) 127821.
[33] J. Yan, S. Wu, C. Yang, Z. Zhao, J. Xie, Influencing mechanisms of RO phase on the cementitious properties of steel slag powder, Constr. Build. Mater. 350 (2022) 128926.
[34] Ministry of Transport of the People's Republic of China (Mot). Technical Guidelines for Construction of Highway Roadbases: JTG/T F20-2015, 2015.
[35] Ministry of Transport of the People's Republic of China (Mot), Test Methods of Materials Stabilized with Inorganic Binders for Highway Engineering, JTG E (2010) 51–2009.
[36] Y. Peng, X. Ou, X. Chen, X. Lin, X. Shen, Utilization of discarded bauxite tailings into eco-friendly foamed mixture lightweight soil, J. Clean. Prod. 333 (2022) 130167.
[37] State Environmental Protection Administration of China. Solid Waste-Extraction Procedure for Leaching Toxicity-Sulphuric Acid & Nitric Acid Method: HJ/T299-2007, 2007.
[38] E.K. Anastasiou, A. Liapis, I. Papayianni, Comparative life cycle assessment of concrete road pavements using industrial by-products as alternative materials, Resour., Conserv. Recycl. 101 (2015) 1–8.
[39] S. Zhang, D. Niu, Hydration and mechanical properties of cement-steel slag system incorporating different activators, Constr. Build. Mater. 363 (2023) 129981.
[40] J. Zhao, Z. Li, D. Wang, P. Yan, L. Luo, H. Zhang, H. Zhang, X. Gu, Hydration superposition effect and mechanism of steel slag powder and granulated blast furnace slag powder, Constr. Build. Mater. 366 (2023) 130101.
[41] G. Ye, X. Liu, G. De Schutter, A.M. Poppe, L. Taerwe, Influence of limestone powder used as filler in SCC on hydration and microstructure of cement pastes, Cem. Concr. Compos. 29 (2) (2007) 94–102.
[42] F. Zhou, H. Meng, G. Pan, R. Mi, Influence of CSH grown in situ on steel slag powder on the performance of fresh and hardened cement pastes, Constr. Build. Mater. 344 (2022) 128269.
[43] R. Duval, Effect of ultrafine particles on heat of hydration of cement mortars, Mater. J. 99 (2) (2002) 138–142.
[44] Z. Chen, S. Wu, Y. Xiao, W. Zeng, M. Yi, J. Wan, Effect of hydration and silicone resin on basic oxygen furnace slag and its asphalt mixture, J. Clean. Prod. 112 (2016) 392–400.
[45] Z. Chen, Z. Leng, Y. Jiao, F. Xu, J. Lin, H. Wang, J. Cai, L. Zhu, Y. Zhang, N. Feng, Y. Dong, Y. Zhang, Innovative use of industrially produced steel slag powders in asphalt mixture to replace mineral fillers, J. Clean. Prod. 344 (2022) 131124.

[46] M. Li, H. Tan, X. He, S. Jian, G. Li, J. Zhang, X. Deng, X. Lin, Enhancement in compressive strength of foamed concrete by ultra-fine slag, Cem. Concr. Compos. 138 (2023) 104954.
[47] T.T. Nguyen, H.H. Bui, T.D. Ngo, G.D. Nguyen, M.U. Kreher, F. Darve, A micromechanical investigation for the effects of pore size and its distribution on geopolymer foam concrete under uniaxial compression, Eng. Fract. Mech. 209 (2019) 228–244.
[48] General Administration of Quality Supervision, Inspection and Quarantine of the People's Republic of China. Standard for Groundwater Quality: GB/T 14848-2017, 2017.